PROCEEDINGS, Eleventh Workshop on Geothermal Reservoir Engineering
Stanford University, Stanford, California, January 21-23, 1986
SGP-TR-93

Quantitative Model of the Cerro Prieto Field

S. E. Halfman, M. J. Lippmann, and G. S. Bodvarsson

Lawrence Berkeley Laboratory
Earth Sciences Division
University of California
Berkeley, California 94720

ABSTRACT

A three-dimensional model of the Cerro Prieto geothermal field, Mexico, is under development. It is based on an updated version of LBL's hydrogeologic model of the field. It takes into account major faults and their effects on fluid and heat flow in the system. First, the field under natural state conditions is modeled. The results of this model match reasonably well observed pressure and temperature distributions. Then, a preliminary simulation of the early exploitation of the field is performed.

The results show that the fluid in Cerro Prieto under natural state conditions moves primarily from east to west, rising along a major normal fault (Fault H). Horizontal fluid and heat flow occurs in a shallower region in the western part of the field due to the presence of permeable intergranular layers. Estimates of permeabilities in major aquifers are obtained, and the strength of the heat source feeding the hydrothermal system is determined.

INTRODUCTION

The Cerro Prieto geothermal field is located in the southern part of the Salton Trough--about 20 miles south of the United States-Mexico border in Baja California, Mexico (Fig. 1). Approximately, 140 deep wells have been drilled in the area (Fig. 2); the wells produce from three major aquifers (α, β and γ reservoirs). To date, the installed electrical power generating capacity at the field is 400 MWe; by the end of 1986 it is expected to reach 620 MWe. A reliable model of the field is needed to assess its ultimate generating potential and to optimize the reservoir exploitation strategy. The model must consider the pre-exploitation conditions of the system and be able to predict reservoir pressure and temperature changes during fluid production. This paper presents preliminary results of a three-dimensional numerical simulation of the pre-exploitation and early production states of the Cerro Prieto field.

The basis for the three-dimensional numerical model presented here is an updated version of Halfman et al.'s (1984) hydrogeologic model that depicts preproduction subsurface geothermal fluid flow patterns in the Cerro Prieto field (Fig. 3). This model explains the role of layers of different permeabilities (i.e., sandstones, sandy shales, and shales) and the effects of major faults on fluid flow. According to Halfman's model, the hot fluids originate at great depths in the eastern portion of the field flowing through the deepest reservoir identified up to now (the γ reservoir; not shown in Fig. 3). Then the fluids

(1) rise along Fault H,
(2) flow westward through the Z sandstone (between wells M-117 and M-123) corresponding to the β reservoir,
(3) ascend into a sandy gap in the O shale (in the vicinity of M-10),
(4) flow westward through a sandy shale layer within the O shale [between M-14 and M-25 (1200-1400 m)] corresponding to the α reservoir,
(5) rise up Fault L, and
(6) flow westward through the shallower sandstone [between M-29 and M-9 (800 - 1000 m)].

Eventually the geothermal fluids either mixes with the cold water surrounding the geothermal anomaly or discharge to the surface in mudpots, fumaroles, hot springs, and hot pools. These postulated fluid flow patterns are consistent with mineralogic (Elders et al., 1981, 1984), thermal (Mercado, 1976), and reservoir engineering and geochemical (Grant et al., 1984) studies conducted on the Cerro Prieto field.

Lippmann and Bodvarsson (1983) developed a two-dimensional numerical model of the field that was based on a portion of Halfman et al.'s (1984) hydrogeologic model. They obtained a good match with the observed natural-state pressures and temperatures. However, because of the two-dimensional nature of the model (not allowing recharge of the system along a horizontal direction perpendicular to the cross section), a good match with reported 1973-1979 pressures was not possible. The three-dimensional model presented here extends the Lippmann and Bodvarsson's (1983) model to three dimensions, thereby not restricting the recharge to the produced reservoir. First, a natural-state model of the field will be discussed, giving estimates for the mass and heat flow and for the permeability distributions in the system. Then, using the same model preliminary results of reservoir behavior under exploitation will be described.

METHODOLOGY

A natural steady-state model of Cerro Prieto was developed by varying the rock properties and boundary conditions of the model until reasonable matches between calculated and observed temperatures (Navarro et al., 1982; Rivera et al., 1982) and pressures (Ayuso, 1984) were obtained. After that, the early (1973-1979) exploitation of the field was simulated to validate the model against the observed reservoir pressure decline (Bermejo et al., 1979).

A three-dimensional, multi-phase, multi-component simulator MULKOM (Pruess, 1983) was used to compute the heat and mass flow in the system.

Computational Mesh

The three-dimensional mesh used in this study was designed on the basis of the geologic characteristics of the field. One side of the model is oriented in a NW-SE direction along the approximate strike of Fault L (Fig. 4). The SW-NE side of model is parallel to Fault H. Both of these faults are important features in the hydrogeological model of Cerro Prieto (Halfman et al., 1984). In plan view, the region modeled extends over an area of 8600 m (SW-NE) by 9000 m (NW-SE). The thickness of the model varies, considering depths between 800 and 4000 m. The mesh consists of 242 elements: 146 internal elements and 96 boundary blocks.

Figure 5 shows the computational mesh for a SW-NE cross section in the upthrown block. The elements are designed to reproduce schematically the geology and characteristics of the various layers comprising the system. The region modeled is below 800 m depth; the shale layer above 800 m is assumed to be impermeable. In general, the lateral boundaries are also assumed impermeable. The recharge of hot fluids is modeled by injection into the mesh elements representing the deep γ reservoir. The discharge of the fluids is through boundary elements located along the western margin of the grid, at 800 m depth. We also assume that the rocks below the β reservoir are of low permeability, except for the sandy γ reservoir. Similar assumptions are made for the corresponding downthrown block.

Material Properties

Different material properties were assigned to various zones in the mesh (Figs. 6A and 6B). In the early simulations, we used values for rock densities, porosities, permeabilities, and heat conductivities similar to those defined from the modeling work of Lippmann and Bodvarsson (1983). Later on, during the matching process with observed temperatures and pressures, the material properties (especially permeablities and thermal conductivities) were adjusted somewhat. Those used in the "best" model are given in Table 1.

Figure 6A shows the materials used in the cross section given in Figure 5. The K1 zone represents the thick sandstones lying to the west of the main geothermal anomaly. The S1 zone is the cooler aquifer overlying the α and β reservoirs. The C1 zone is a leaky caprock to the α reservoir (S2 zone). The relatively low permeability C2 zone separates the α and β reservoir in the western portion of the field. The F1 zone corresponds to Fault L. The S3 and S3B zones are the β reservoir in the western portion of the field. S4 is a sandy zone overlying the C4 zone which is the caprock to the sandy β reservoir (S5 zone) in the eastern portion of the field. The C5 is a low-permeability zone due to mineral precipitation in the upper part of the sandy gap (S7 zone). C6 is a shaly zone separating the β reservoir from the sandy γ reservoir (S6 zone).

Figure 6B shows the zones (materials) in a cross section along a SW-NE downthrown row of elements. The K1 and S1 sandstones are equivalents to those of the upthrown block. A new C7 shaly zone is identified in this cross section because no α reservoir exists in this area of the downthrown block. A shale zone (C8) is arbitrarily assigned to part of this section because of lack of well data in the area. The rest of the zones in this section are similar to those of the upthrown section (Fig. 6A).

The result of our model indicates that the permeabilty of the shale layers varies generally between 0.005 and 1 md, and that of the sandy materials between 1 and 100 md. In the three reservoirs (α, β, and γ), the horizontal permeability is 100 md and the vertical permeability ranges between 1 and 10 md. These values agree reasonably well with the results of well tests and with permeabilities used in earlier simulations of the field (Lippmann and Bodvarsson, 1983; Ayuso, 1984).

A thermal conductivity of 2.0 W/m °C is used for the different zones except for a few zones where it is slightly higher. A constant rock density of 2,650 kg/m^3 is assumed for all materials.

Boundary Conditions

In our model, boundary elements are located along the west, north, and top sides. Conductive heat transfer is allowed from all boundary elements. The temperatures for these elements were selected on basis of temperature log data (Bermejo et al., 1979; and Bermejo, personal communication, 1982). Five of the boundary elements located along the western edge on the top row were open to fluid flow. The constant pressure for the fault and two upthrown open boundary elements is 68 bars and those for the two downthrown open boundary elements are 100.3 and 101.1 bars, respectively. For the best model, a constant rate of hot fluid recharge of 100 kg/s is assumed in the γ reservoir along the eastern edge of the model.

Natural State Model

The natural state model describes the heat and fluid flows, and the distribution of pressures, temperatures, and steam saturations in the system before commercial

fluid production is initiated. The model discussed in this paper is the one that presently best matches the field data.

The properties of the different zones in this "best" model are given in Table 1. The total rate of hot (1512 kJ/kg) water recharge along the eastern side of the model is about 100 kg/s. Figures 7A and 7B show the observed and computed isotherms respectively, for the SW-NE cross section shown in Figure 5. In the eastern portion of the field (east of the sandy gap), there is a good temperature match. The isotherms between 150° to almost 300° C indicate a high-temperature gradient in the caprock (hatched zone). As the hot fluids ascend through the sandy gap in the caprock, the isotherms rise to shallower depths, as is confirmed by the field data. In the western part of the cross section (west of sandy gap) the agreement between observed and computed temperatures is not as good; the computed ones are generally too high (about 50° C).

The discrepancies in the western region may be due partly to two factors. First, the field temperatures used reflect temperatures more closely associated to those found along cross section A-A' of Halfman et al.'s (1984). This section is about 1000 m northwest of the section shown in Figures 7A and 7B. There is evidence that a few wells such as M-181 are hotter, especially west of Fault L. This suggests that the temperatures given in Figure 7A should be somewhat higher towards the west.

The second and probably more accurate reason for the temperature discrepancy along the western region is the existence of cold water recharge between 1200 and 1400 m depth along the western margin of the field (Lippmann and Bodvarsson, 1983). This recharge was not considered in the model discussed here; it will be taken into account in our future modeling work.

The temperature distribution at 1300 and 1750 m depth are given in Figures 8 and 9, respectively. Figures 8A and 9A show observed values as reported by Navarro et al. (1982); Figure 8B and 9B are the computed ones. For the temperatures at 1300 m there is a reasonable match. East of the railroad tracks, the regions between isotherms are narrow, reflecting the presence of Fault H that controls the upflow of hot fluids. West of the tracks, the isotherms spread out; in a N-S direction (Fig. 8A) and in a NW-SE direction (Fig. 8B). The main difference between observed and calculated temperatures is that the computed temperature distribution along the western edge of the field is spread over a wider area than that shown on Figure 8A. One could argue that the actual temperature distribution in this part of the field is not well known because of a scarcity of well data. However, an alternate possibility is natural cold water inflow along the western margin of the field; this will be tested in future simulations.

Figure 9A shows the observed temperatures at 1750 m depth. East of the railroad tracks the 150° and 100° C isotherms are not given. Ignoring the corresponding two contours in Figure 9B, in the eastern region the calculated and observed temperature contours show a similar trend of converging towards Fault H. West of the tracks, both the observed and calculated isotherms show a general trend of spreading, in an N-S direction (Fig. 9A) and in a NW-SE direction (Fig. 9B). However, the observed temperature contours delineate a smaller region and show a distinct elongation to the SW which is not shown in Figure 9B. The differences between observed and calculated temperatures can again be explained by the scarcity of data or by cold water inflow. There is very limited well data for the western region of the field, especially below a depth of 1750 m. An influx of colder waters, if included in our model, could improve the match between observed and computed temperatures.

Table 2 shows some comparisons of observed pressures (Ayuso, 1984), calculated pressures from Lippmann and Bodvarsson's (1983) two-dimensional modeling study, and our calculated pressures. In the α and the western β reservoirs, the calculated pressures are lower (6 and 13 bars, respectively) than those computed by Lippmann and Bodvarsson's (1983). Our calculated pressures should increase somewhat when cold water recharge from the west is added to the model. In the section modeling Fault H the calculated pressure agrees well with the observed pressure. In the eastern β reservoir, the calculated pressure is 4.5 bars higher than the one reported by Ayuso (1984).

From Halfman et al.'s (1984) hydrogeologic model, it was concluded that the general geothermal fluid flow pattern is from large depths in the east to shallower depths in the west, and that some of the hot fluids escape to the surface along the western margin of the field. Our three-dimensional model essentially shows the same flow pattern (e.g., Fig. 10). Hot fluid enters the system through the γ reservoir in the east. The fluid moves westward and then up Fault H into the Z sandstone (β reservoir) where it slightly spreads to the NE and SW. Then, the fluid in the Z sandstone flows predominately westward. In the vicinity of the sandy gap, most of the fluid in the model is either flowing through the SW-NE upthrown row of elements next to or in Fault H zone, itself. A good portion of the fluid rises up the sandy gap, then flows westward into the α reservoir, up Fault L, and westward in the shallow sandstone aquifer and out the model through the top western elements. Because of the three-dimensional nature of the model, the fluid flow pattern shown on Figure 10 is only schematic. Perpendicular to this cross section there is also some fluid movement especially from the Fault H zone, located to the SE, and at the western edge of the section from the sandy region (zone K1).

Production Model

As part of the validation of our three-dimensional model of Cerro Prieto we simulated the exploitation of the α reservoir from 1973 to the end of 1979. At this stage, we assumed yearly constant production rates.

For the period considered, the flow rates were 345, 590, 603, 695, 751, and 716 kg/sec. In Figure 11 the agreement between computed and observed α reservoir pressures is quite reasonable. This is very encouraging since it indicates that the physical parameters assumed for the model, especially for the α reservoir, are generally correct. As we improve the natural state model of the field we expect to obtain a better match with the pressures reported by Bermejo et al. (1979).

CONCLUSIONS

A three-dimensional model of Cerro Prieto is under development. For pre-exploitation conditions the model gives fluid flow patterns consistent with those of Halfman et al. (1984). The calculated and observed temperature distributions match reasonably well. The computed pressures are somewhat lower than the observed ones. The computed pressure drawdown in the α reservoir also matches well with the observed 1973-1979 pressure decline. We expect to improve the agreement between observed and computed data by refining our three-dimensional model and by including in the calculation cold water recharge along the edges of the field. These future improvements of the model will allow its use for predicting the behavior of Cerro Prieto as fluid production is expanded to the eastern areas and to deeper reservoirs.

ACKNOWLEDGEMENTS

We thank our colleagues of the Comisión Federal de Electricidad for providing the data used in this study. This work was supported by the Assistant Secretary for Conservation and Renewable Energy, Office of Renewable Technology, Division of Geothermal Technology of the U. S. Department of Energy, under Contract No. DE-AC03-76SF00098.

REFERENCES

Ayuso, M. A., 1984. Gerencia de Proyectos Geotermoeléctricos, Com. Fed. de Electr. internal report 1384-027 and 028, Departamento de Evaluación y Yacimientos, 15 p.

Bermejo, M., F. J., F. X. Navarro O., F. Castillo B., C.A. Esquer, and C. Cortez A., 1979. Pressure variations at the Cerro Prieto reservoir during production, in Proceedings, Second Symposium on the Cerro Prieto Geothermal Field, Com. Fed. de Electr. Mexicali, Mexico, Oct. 17-19, 1979, pp. 473-493.

Elders, W. A., A. E. Williams, D. A. Bird, and P. Schiffman, 1984. Hydrothermal flow regime and magmatic heat source of the Cerro Prieto geothermal system, Baja California, Mexico, Geothermics, v. 13, p. 27-47.

Elders, W. A., A. E. Williams, and J. R. Hoagland, 1981. An integrated model for the natural flow regime in the Cerro Prieto hydrothermal system based upon petrological and isotope geochemical criteria, in Proceedings, Third Symposium on the Cerro Prieto geothermal field, March 24-26, 1981, San Francisco, California; Lawrence Berkeley Laboratory Report LBL-11967, pp. 102-109.

Grant, M. A., A. H. Truesdell, and A. Mañón, 1984. Production induced boiling and cold water entry in the Cerro Prieto geothermal reservoir indicated by chemical and physical measurements, Geothermics, v. 13, pp. 117-140.

Halfman, S. E., M. J. Lippmann, R. Zelwer, and J. H. Howard, 1984. A geologic interpretation of the geothermal fluid movement in Cerro Prieto field, Baja California, Mexico, Assoc. Pet. Geol. Bull., v. 68, pp. 18-30.

Lippmann, M. J., and G. S. Bodvarsson, 1983. Numerical studies of the heat and mass transport in the Cerro Prieto geothermal field, Mexico, Water Resources Research, v. 19, no. 3, pp. 753-767.

Mercado, G. S., 1976. Movement of geothermal fluids and temperature distribution in the Cerro Prieto geothermal field, in Proceedings, Second United Nations Symposium on the Development and Use of Geothermal Resources, May 20-29, 1975, Washington, D.C., U.S., Government Printing Office, v. 1, pp. 489-494.

Navarro, F.X., F. J. Bermejo, F. Castillo, and R. Rivera, 1982. Update of temperature behavior and distribution in Cerro Prieto I, in Proceedings, Fourth Symposium on the Cerro Prieto Geothermal Field, Com. Fed. de Electr., Guadalajara, Mexico, Aug. 10-12, 1982, pp. 81-91.

Pruess, K., 1983. Development of the general purpose simulator MULKOM, in 1982 Annual Report Earth Sci. Div., Lawrence Berkeley Laboratory report LBL-15500, pp. 133-134.

Rivera, R. J., F. Bermejo, F., Castillo, H. Pérez, and A. Abrajān, 1982. Update of the temperature behavior and distribution in Cerro Prieto II and III, in Proceedings, Fourth Symposium on the Cerro Prieto Geothermal Field, Com. Fed. de Elect., Guadalajara, Mexico, August 10-12, 1982, pp. 93-112.

Table 1. Properties of the materials assigned to the zones used in the model, as shown in Figure 6A and 6B.

Zones	Porosity (%)	Permeability (md) x	y	z
K1,S1,S2,S3,S4	16	100	100	10
S3B,S5,S6	14	100	100	1
S7	14	100	10	10
C1,C2	22	1	1	0.1
C4,C5,C6,C7,C8	25	.5	.005	.005
F1	14	50	50	50

Table 2. Natural state model validation. Pressure comparisons.

Region	Depth (m)	Pressure (bars)		
		Observed Ayuso(1984)	Calculated (Lippmann & Bodvarsson, 1983)	Calculated in this study
α reservoir	1300	-	118.8	112.8
β reservoir (west of sandy gap)	1700	-	156.0	143.5
Fault H	2600-2900	235	-	233.8
β reservoir (east of sandy gap)	2500-2840	228	-	232.5

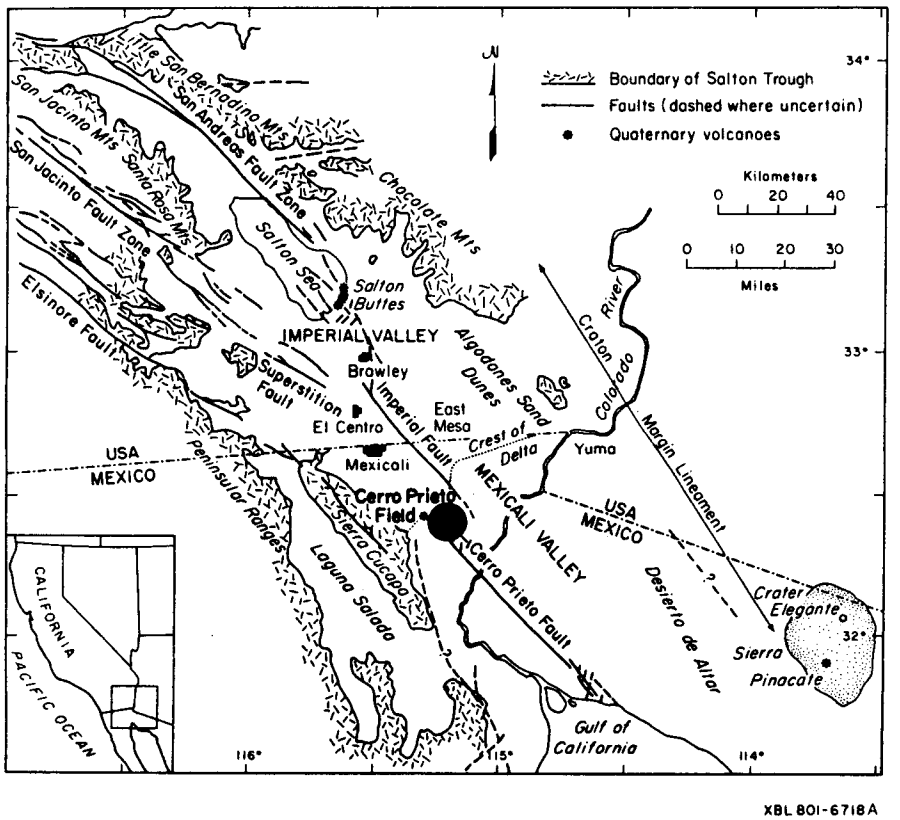

Figure 1. Regional geology of Salton Trough (i.e., Imperial and Mexicali Valleys) and location of the Cerro Prieto field.

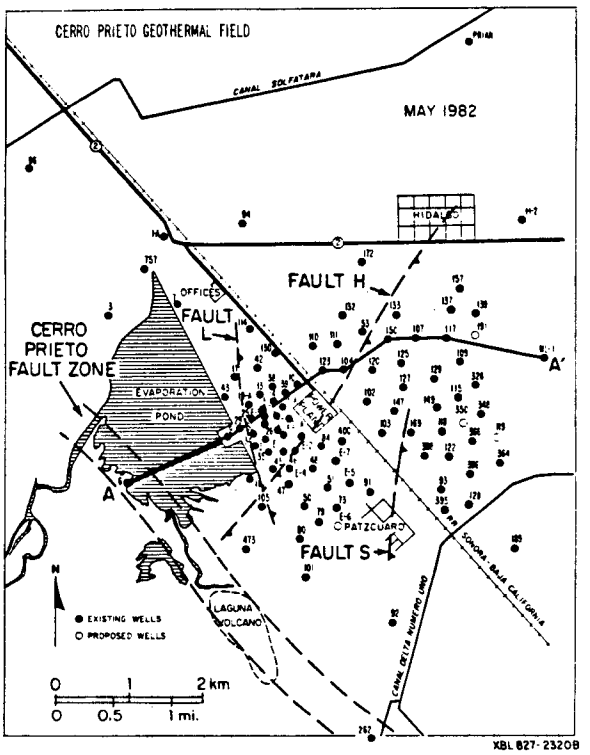

Figure 2. Location of some of the wells, principal faults, and cross section A-A' at Cerro Prieto.

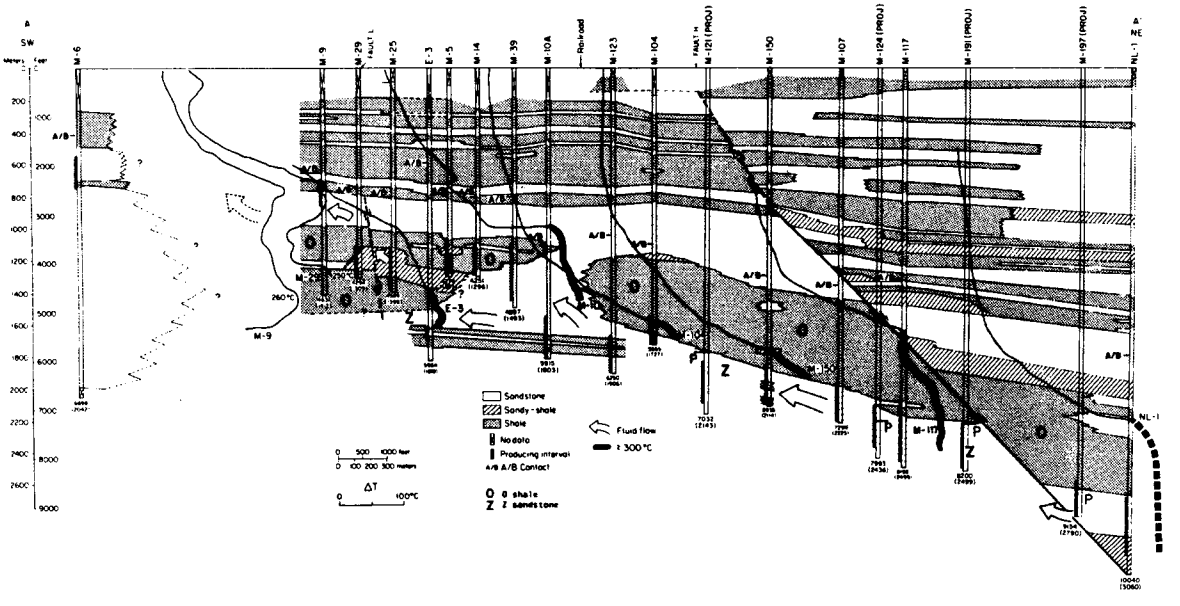

Figure 3. Lithofacies cross section A-A', showing well locations, lithofacies groups, faults, temperature profiles, producing intervals, A/B contacts, shale unit O, sand unit Z, and arrows indicating direction of fluid flow. On temperature profiles, points corresponding to 300 ° C are placed under the location of the respective wells. Parts of temperature profiles shown by heavy lines indicate temperatures 300 ° C or higher.

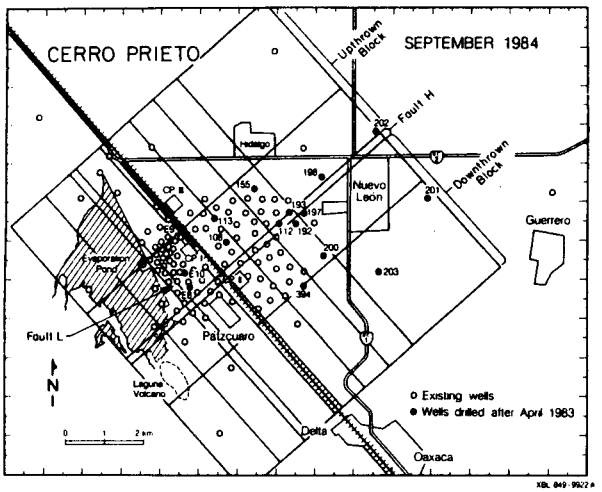

Figure 4. Plan view of the computational mesh used in the work.

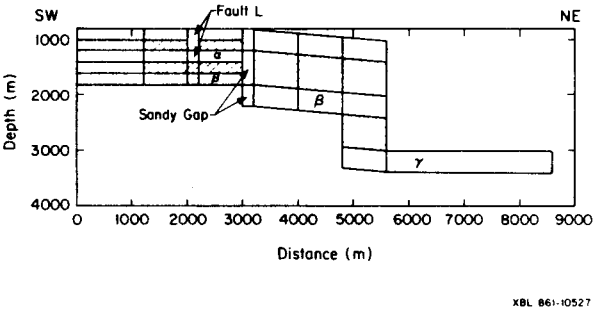

Figure 5. Cross section through the SW-NE row of elements just north of the Fault H. Grid elements are shown, hatched zones represent layers of lower permeability.

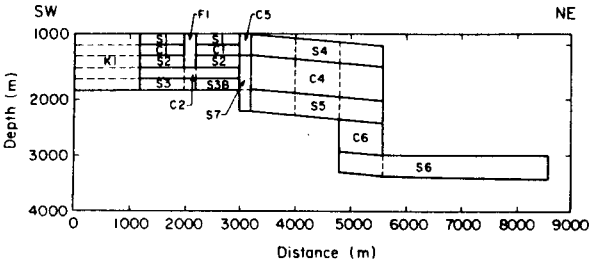

Figure 6A. Cross section given in Figure 5 showing different materials used for the upthrown block.

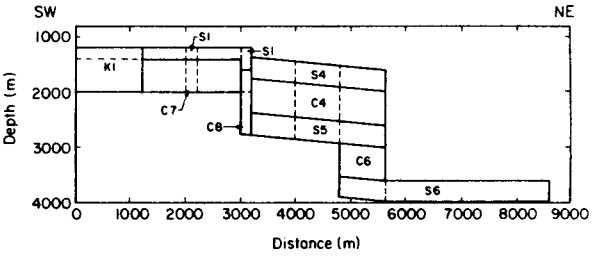

Figure 6B. Cross section through the southernmost SW-NE row of elements representing different materials used for the downthrown blocks.

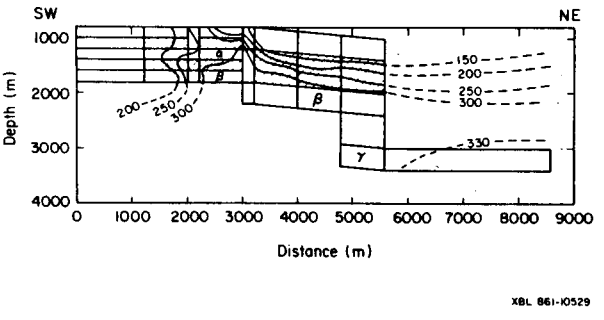

Figure 7A. Cross section given in Figure 5 showing observed temperature distribution (° C).

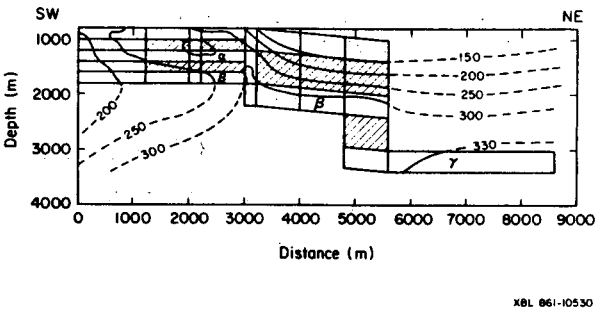

Figure 7B. Cross section given in Figure 5 showing calculated temperature distribution (° C).

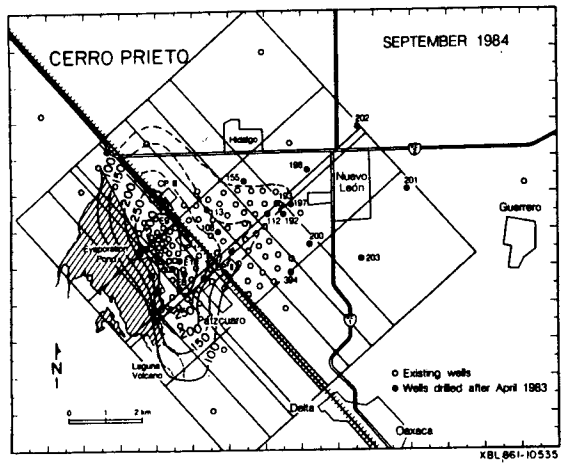

Figure 8A. Observed temperature distribution (° C) at 1300 m depth (Navarro, et al., 1982).

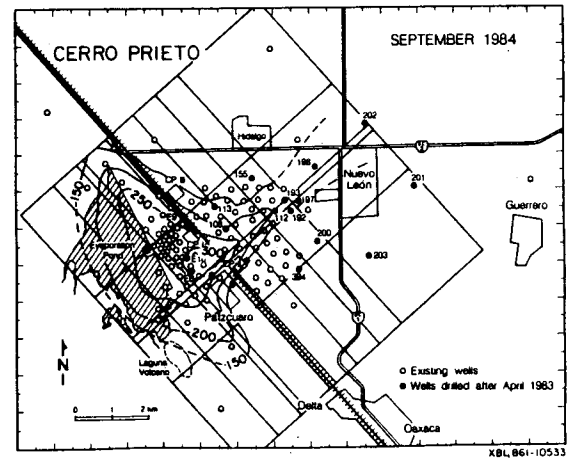

Figure 8B. Calculated temperature distribution (° C) at 1300 m depth.

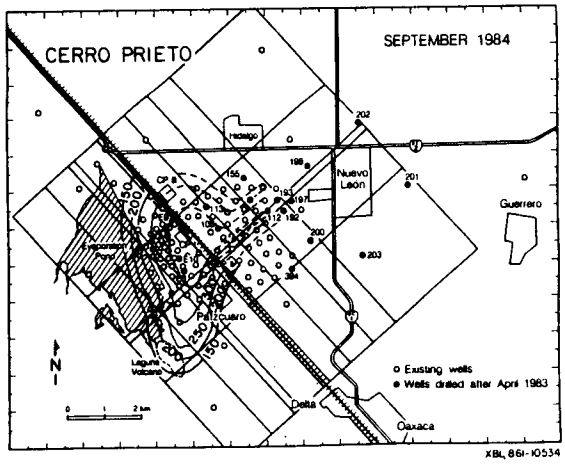

Figure 9A. Observed temperature distribution (° C) at 1750 m depth (Navarro et al., 1982).

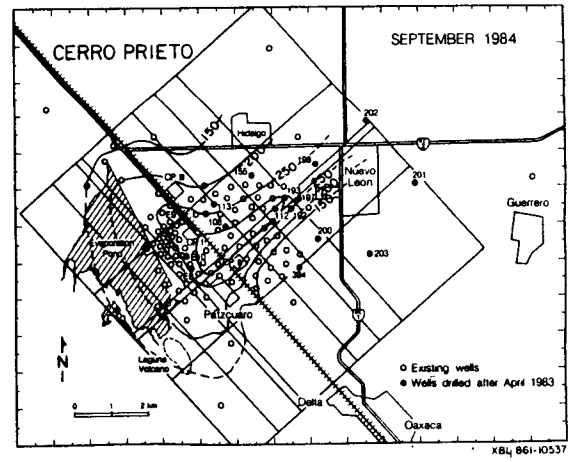

Figure 9B. Calculated temperature distribution at 1750 m depth.

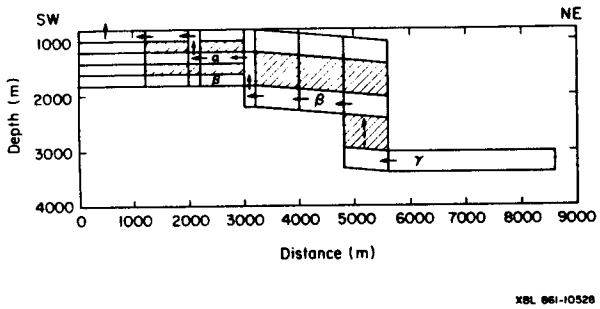

Figure 10. Generalized fluid flow pattern for the cross section shown in Figure 5. The dashed arrow between the β and γ reservoirs indicates vertical flow in the fault zone (located to the southeast).

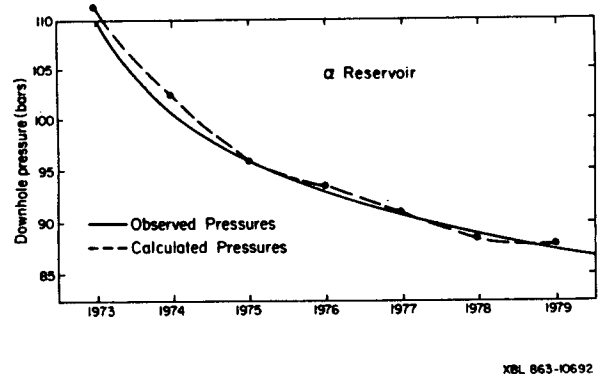

Figure 11. Comparisons of observed (Bermejo et al., 1979) and calculated pressure changes (in bars) in the α reservoir.